Effect of dislocation core fields on discrete dislocation plasticity

Irani, Nilgoon; Murugesan, Yaswanth; Ayas, Can; Nicola, Lucia

Important note
To cite this publication, please use the final published version (if applicable).
Please check the document version above.

Research paper

Effect of dislocation core fields on discrete dislocation plasticity

Nilgoon Irani [a,1], Yaswanth Murugesan [b,1], Can Ayas [a], Lucia Nicola [a,b,*]

[a] *Faculty of Mechanical, Maritime, Materials Engineering, Delft University of Technology, 2628 CD Delft, The Netherlands*
[b] *Department of Industrial Engineering, University of Padova, I-35131, Italy*

ARTICLE INFO

ABSTRACT

Discrete dislocation plasticity is a modeling technique that treats plasticity as the collective motion of dislocations. The dislocations are described through their elastic Volterra fields, outside of a cylindrical core region, with a few Burgers vectors of diameter. The contribution of the core fields to the dislocation dynamics is neglected, because it is assumed that their range is too short to be of influence. The aim of this work is to assess the validity of this assumption.

In recent ab-initio studies it has been demonstrated that the dislocation core fields are significant up to a distance of ten Burgers vector from the dislocation line. This is a longer range influence than expected and can give rise to changes in the evolving dislocation structure and in the overall response of a plastically deforming body. It is indeed experimentally observed that dislocations pile up against strong interfaces, and that the spacing between dislocations at the front of these pile-ups can be less than ten Burgers vectors.

In this work, 2-D discrete dislocation plasticity simulations are performed to investigate the effect of core fields on edge dislocation interactions. The results of the simulations, which include core fields for the first time, show indeed that dislocations that are very closely spaced experience additional glide or climb due to core fields. The effect is however negligible when compared to glide and climb due to Volterra fields or due to the external load.

1. Introduction

Discrete dislocation plasticity (DDP) simulation is a numerical technique appropriate to model the plastic behavior of metals at the micrometer scale (Kubin et al., 1992; der Giessen and Needleman, 1995; Ghoniem and Sun, 1999; Ghoniem et al., 2000; Weygand et al., 2002; Amodeo and Ghoniem, 1990). It helped to shed light on plasticity size effects in thin films (Nicola et al., 2006, 2003; Ayas et al., 2012; Venugopalan and Nicola, 2019), micropillars (Wei et al., 2019; Huang et al., 2017; Chang et al., 2016; Fan et al., 2012), contact deformation (Fivel et al., 1997; Zhang et al., 2014), crack-growth under monotonic and cyclic loading (Shin et al., 2005; Reddy et al., 2013; Deshpande et al., 2003), and the climb assisted formation of dislocation cell structures (Wu and Zaiser, 2020; Xia and El-Azab, 2015). In DDP simulations, plasticity is modeled as the collective motion of discrete dislocations that are described through the Volterra elastic fields in an otherwise continuum domain Hirth and Lothe (1968). It is however well-known that the dislocation fields deviate from the elastic Volterra description for distances smaller than few atomic spacings from the dislocation line, due to the non-linearities and perturbations associated to the atomic nature of the dislocation (Eshelby et al., 1953; Clouet

et al., 2009). The DDP simulations performed until now used the Volterra fields with a cut-off at the core and neglected the fields a dislocation core might exert on neighboring dislocations. The Volterra fields are used, along with their image fields, to compute the Peach–Koehler force which controls the dislocation dynamics. The core fields are neglected, following the assumption that their field of influence is too short-ranged to affect significantly the evolution of the dislocation structure and therefore the global mechanical response of the solid. The goal of this work is to test the validity of this assumption, by performing 2-D DDP simulations with and without core fields on selected cases.

It is experimentally observed that dislocations form long pile-ups against the barriers along their path, such as grain or phase boundaries and precipitates. The dislocations at the front of the pile-up can be very densely packed. They exert both a stress at the barrier against which they pile up and a long range back-stress. The back-stress has opposite sign to the resolved shear stress that gave rise to the pile-up itself, and often hinders the further nucleation of dislocations from the dislocation source, leading to strain hardening of the material (Yang et al., 2016). Given the importance of pile-ups in determining the plastic response of micron-scale objects, it is of importance to analyze

whether neglecting core fields in the computation of the Peach–Koehler force in DDP simulations affects the dislocation structure. Specifically, core fields of neighboring dislocations might contribute to additional glide of the dislocations in a pile-up but, even more importantly, to their climb on different planes. A change in the length and density of pile-ups might have an impact on the global response of the metal crystal at room or high temperature. Dislocation climb has been included in two-dimensional discrete dislocation plasticity simulations (2D-DDP) (Davoudi et al., 2012; Danas and Deshpande, 2013; Ayas et al., 2014, 2015) and has resulted in a softer material response and less pronounced size effects. In recent years, several ab-initio studies considered the effect of the dislocation core through EAM potentials (Clouet et al., 2009; Henager and Hoagland, 2000, 2005; Walker et al., 2005a,b; Clouet, 2011). These studies showed that when subtracting fields of the Volterra contribution from the ab-initio calculations, one obtains a closed-form residual dislocation core field. Henager and Hoagland (2005) found that for separation distances between dislocations even up to $50b$ (where b is the magnitude of Burgers vector) the core fields are comparable to the Volterra fields. The study of Kuan and Hirth (1976) suggested that the equilibrium spacing between dislocations in a pile-up and the stress fields at the head of a pile-up are affected by the dislocation core fields. Their numerical investigation on the behavior of dislocation pile-ups at the interface of a bi-material couple revealed that by including the effects of dislocation core in the computation of dislocation interactions, the spacing between the dislocations is reduced around the tip of a pile-up. As a consequence, the stress concentration at the tip of the pile-up is slightly enhanced.

Core effects in the plastic deformation of an FCC crystal might arise from full or partial dislocation core (Wei and Peng, 2017; Peng et al., 2019). Herein we will focus on full dislocations, because considering the presence and motion of partials is not appropriate in the 2D-DDP framework. The plane of analysis in 2D-DDP is the (110) plane of the FCC crystal, the only plane where straight dislocations can glide and give the same slip traces that would be provided by slip on a three-dimensional FCC crystal (Rice, 1987), while partials have a Burgers vector $< a/6(112) >$ and move on the {111} plane. This means that neither the Burgers vector nor the slip direction would be contained in the plane of analysis of the simulations. The two-dimensional simulations, moreover, have as the main scope to track the collective motion of the discrete dislocations which provide plasticity. The presence and motion of dislocation partials are expected to have a negligible effect in the plastic response of the solids studied with 2D-DDP.

Herein, we only consider the core effects from the straight full dislocations that nucleate and glide on the $\langle 110 \rangle$ direction of an FCC crystal. To this end, we perform simulations including the analytical expressions for the core fields derived by Henager and Hoagland (2005), who represented the core fields in a linear-elastic continuum framework as cylindrical dilatations caused by a line defect. This line defect is represented by unequal force dipoles. The representation is a generalization of the one proposed by Nabarro (1967), who considered the core as the center of dilatation with cylindrical symmetry: the long-range field corresponding to these couples is equivalent to that produced by a two-dimensional elliptical inclusion inserted into a circular hole.

2. Elastic core fields of dislocations

The core of a dislocation produces a net dilatation of the linear elastic isotropic continuum in which the dislocation is embedded (Gehlen et al., 1972). Following Henager and Hoagland (2005), this expansion is modeled by a pair of unequal force couples without moments (refer to Fig. 1), which act at the dislocation line. The corresponding long-range linear elastic displacement fields are

$$\tilde{u}_1^{\text{Core}} = \frac{M_2 \cos(\theta)}{4\pi\mu r} [2\alpha(1-\beta) + \beta(\alpha-1)\cos(2\theta)],$$
$$\tilde{u}_2^{\text{Core}} = \frac{M_2 \sin(\theta)}{4\pi\mu r} [2(1-\beta) + \beta(\alpha-1)\cos(2\theta)].$$
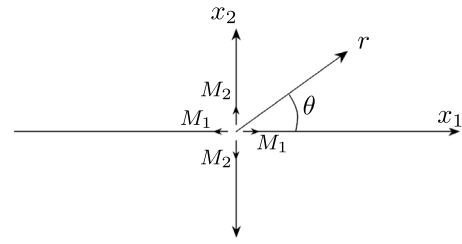
(1)

Fig. 1. Pair of orthogonal force couples used to represent the core of a dislocation.

Here, $M_1(\text{N})$, $M_2(\text{N})$ are the forces in the couples acting along the x_1 and x_2 directions, respectively and α is the ratio M_1/M_2. The material point at which the fields are computed is identified by vector r, with $\theta = \tan^{-1}(x_2/x_1)$. The elastic properties of the medium where the dislocations are embedded are the shear modulus μ and the Poisson's ratio v, with $\beta = 1/2(1-v)$. The values of M_1 and M_2 were evaluated by Henager and Hoagland (2005) through comparison with ab-initio calculations. From the core displacements, the core stress fields are determined using linear elasticity

$$\tilde{\sigma}_{11}^{\text{core}} = -\frac{(M_1+M_2)(1-\beta)\cos(2\theta)}{2\pi r^2} + \frac{(M_2-M_1)\beta(\cos(2\theta)+\cos(4\theta))}{2\pi r^2},$$
$$\tilde{\sigma}_{22}^{\text{core}} = \frac{(M_1+M_2)(1-\beta)\cos(2\theta)}{2\pi r^2} + \frac{(M_2-M_1)\beta(\cos(2\theta)-\cos(4\theta))}{2\pi r^2},$$
$$\tilde{\sigma}_{12}^{\text{core}} = -\frac{(M_1+M_2)(1-\beta)\sin(2\theta)}{2\pi r^2} + \frac{(M_2-M_1)\beta\sin(4\theta)}{2\pi r^2}.$$

(2)

In Fig. 2 the normal components of the edge dislocation stress fields are presented, while in Fig. 3a the variation of the normal fields along the positive x_1-axis is shown with and without core contribution. A vector plot of the displacement field from both the core and Volterra contributions are shown in Fig. 3b.

3. 2D-DDP formulation in brief

The goal of discrete dislocation plasticity is to compute at each time increment of the simulation the solution of a boundary value problem for a crystalline metal subject to external loading and containing a given density of dislocations. The displacement, stress field and strain field in the solid are calculated using superposition of: (i) the (˜) fields of the dislocations and (ii) the smooth image (ˆ) fields which ensure that the boundary conditions are satisfied,

$$u_i = \hat{u}_i + \tilde{u}_i, \qquad \varepsilon_{ij} = \hat{\varepsilon}_{ij} + \tilde{\varepsilon}_{ij}, \qquad \sigma_{ij} = \hat{\sigma}_{ij} + \tilde{\sigma}_{ij}.$$

(3)

The image fields are here obtained by solving a linear elastic boundary value problem using the finite element method. The (˜) dislocation fields, instead, are provided by their analytical description. Considering that the dislocation fields are linear elastic the contribution of all the N dislocations at a point can be obtained as a sum over N,

$$\tilde{u}_i = \sum_{I=1}^{N} \tilde{u}_i^{(I)}, \qquad \tilde{\varepsilon}_{ij} = \sum_{I=1}^{N} \tilde{\varepsilon}_{ij}^{(I)}, \qquad \tilde{\sigma}_{ij} = \sum_{I=1}^{N} \tilde{\sigma}_{ij}^{(I)}.$$

(4)

The motion of the dislocations is assumed to be driven by a combination of glide and climb. Following Ayas et al. (2012), we consider the motion of an edge dislocation from location A at time t to location C at time $t+\Delta t$ (see Fig. 4). The displacement from A to C is decomposed into a climb-only, $\bar{u}$, (from location A at time t to location B at time $t+\Delta t_c$) and a glide-only, $\breve{u}$, component (from location B at time $t+\Delta t_c$ to location C at time $t+\Delta t$). The displacement rate $\dot{u}_i$ is calculated as

$$\dot{u}_i = \frac{1}{\Delta t}[\breve{u}_i^{(t+\Delta t)} - \breve{u}_i^{(t)}] + \frac{1}{\Delta t}[\bar{u}_i^{(t)} - \bar{u}_i^{(t+\Delta t_c)}].$$

(5)

In case the motion of the edge dislocation from A to C occurs by first a glide step followed by a climb step, then Eq. (5) needs to be modified
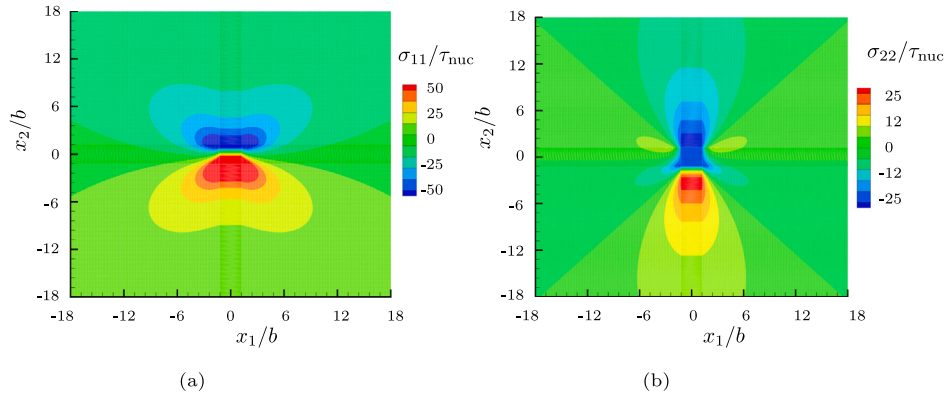
Fig. 2. The stress fields of an edge dislocation in an infinite linear isotropic domain when including both Volterra and core fields: (a) σ_{11}, (b) σ_{22}. The infinite domain is taken to have the elastic properties of aluminum (Henager and Hoagland, 2005).
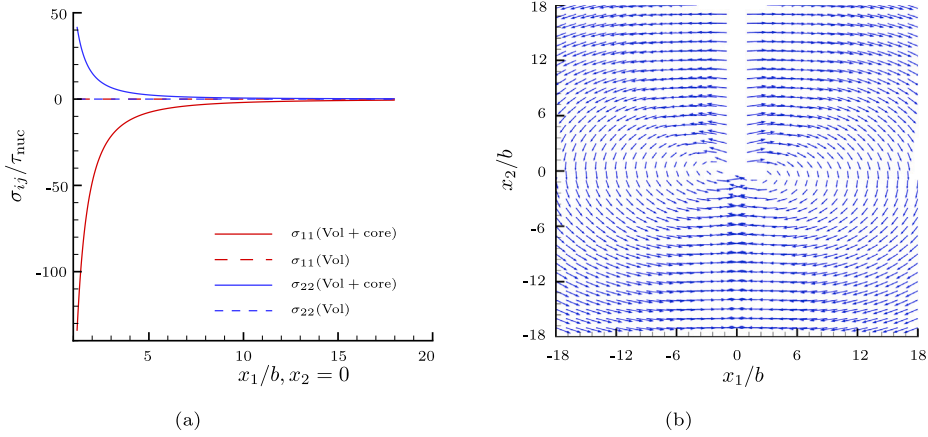

Fig. 3. (a) Normal components of the edge dislocation stress fields with core (Vol+core) and without core (Vol) contribution along the positive x_1-axis, (b) vector plot of the displacement field of an edge dislocation when considering both Volterra and core contributions.

by swapping the order of the $\breve{u}_i$ and $\bar{u}_i$ terms. Within time integration, the order of these events cannot be resolved and hence, the arbitrary assumption we will make is that glide precedes climb when an edge dislocation is gliding in the direction of its Burgers vector whereas the order is reversed when the dislocation glides in the direction opposite to its Burgers vector. This convention ensures no net contribution to $\mathring{u}_i$ is made by vibratory motions of the dislocations. In Eq. (5), the climb components of the displacement field $\bar{u}_i$ are given as

$$\bar{u}_1 = \frac{b}{4}\,\mathrm{sign}(x_1, x_2), \tag{6}$$

$$\bar{u}_2 = 0, \tag{7}$$

where b is the magnitude of the Burgers vector of the edge dislocation, while x_1 and x_2 are the coordinates of the material point measured in the local coordinate system of the dislocation. The main change of the model used in this work, compared to previous climb-assisted dislocation dynamics simulations, is that the component of the displacement field $\breve{u}_i$ in Eq. (5) contains the contribution from core fields in addition to the Volterra fields i.e.,

$$\breve{u}_i = \breve{u}_i^{\mathrm{Vol}} + \breve{u}_i^{\mathrm{Core}}. \tag{8}$$

3.1. Constitutive rules

As typical in discrete dislocation plasticity simulations, the dislocation dynamics are controlled by constitutive rules, inspired by nanoscale phenomena, based on the Peach–Koehler force. The glide and
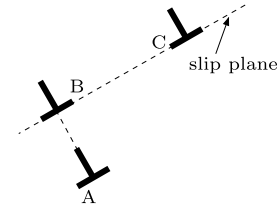

Fig. 4. Sketch of the combined glide and climb of an edge dislocation during its motion from location A at time t to location C at time $t + \Delta t$. The motion involves first climbing to the intermediate location B at time $t + \Delta t_c$ and then gliding to the final position C at time $t + \Delta t$.

climb components of the Peach–Koehler force $f^{(I)}$ on dislocation I are calculated as

$$
\begin{aligned}
f_g^{(I)} &= \left(\hat{\sigma}_{ij} + \sum_{J \neq I} \tilde{\sigma}_{ij}^{(J)} \right) b_j^{(I)} m_i^{(\alpha)}, \\
f_c^{(I)} &= -\left(\hat{\sigma}_{ij} + \sum_{J \neq I} \tilde{\sigma}_{ij}^{(J)} \right) b_j^{(I)} s_i^{(\alpha)},
\end{aligned}
\tag{9}
$$

respectively. The stress field ($\tilde{\sigma}_{ij}^{(J)}$) due to the combined Volterra and core contributions of dislocation J at the position of dislocation I is

$$\tilde{\sigma}_{ij}^{(J)} = \tilde{\sigma}_{ij}^{\mathrm{Vol}} + \tilde{\sigma}_{ij}^{\mathrm{Core}} \tag{10}$$

The Burgers vector of dislocation I is $b_j^{(I)}$. The unit vector normal to slip system α is indicated by $m_i^{(\alpha)}$ and the unit vector in the slip direction is

$s_i^{(\alpha)}$. The glide and climb velocities of dislocation *I* have a linear relation with the glide and climb components of the Peach–Koehler force, albeit with a different drag coefficient:

$$v_g^{(I)} = \frac{1}{B_g} f_g^{(I)}; \quad v_c^{(I)} = \frac{1}{B_c} f_c^{(I)}. \tag{11}$$

Here, new dislocation pairs are generated by Frank–Read sources, mimicked by discrete point sources, randomly distributed in the crystal. Nucleation occurs when the resolved shear stress on a source exceeds $\tau_{nuc} b$ for a time period t_{nuc}. The Burgers vector of the freshly nucleated dislocations is aligned with $s^{(\alpha)}$. Opposite signed dislocations on slip system α annihilate when they are closer than L_e, the critical distance for annihilation.

3.2. Reference parameters

In this work, an isotropic crystal is modeled with Young's modulus $E = 70$ GPa and Poisson's ratio $\nu = 0.33$, representative values for aluminum. The dislocations have a Burgers vector of magnitude $b = 0.25$ nm and the core radius is taken to be twice the Burgers vector, $r_c = 2b$. The core radius is the distance below which the Volterra stress field is cut-off to avoid the singularity typical of an elastic solution.

In all calculations, the crystal is initially dislocation-free. The sources nucleate a dipole when the resolved shear stress acting on them exceeds a critical value of $\tau_{nuc} b$ for a period of time $t_{nuc} = 10$ ns; τ_{nuc} for the sources is taken to have a Gaussian distribution with a mean source strength $\tau_{nuc} = 50$ MPa and a standard deviation of 10 MPa. The drag coefficient for glide B_g is 10^{-4} Pa s. The parameter B_c/B_g which governs the climb rates relative to the glide rates is taken as 10^4. This parameter was chosen following the work of Danas and Deshpande (2013), wherein a numerical expression for the climb coefficient B_c was proposed as a function of temperature, equilibrium vacancy concentration and vacancy diffusion coefficient. The critical distance for annihilation is $L_e = 6b$. A time step of $\Delta t = 0.5$ ns is used to update the dislocation structure. Following Henager and Hoagland (2005), the magnitude of line force couples used for the description of core fields in aluminum are $M_1 = 0.6$ N and $M_2 = 0.3$ N.

3.3. Simulation test cases

To assess the effect of core fields on the evolution of dislocation structures in 2-D DDP simulations, we start with two simple but illustrative case studies where a single dislocation source is active, and the effect of core fields can be most easily identified. Next, we move to a realistic scenario; where a thin layer with multiple active sources and slip systems are loaded in tension.

CASE 1: A dislocation source in an infinite single crystal that is surrounded with impenetrable boundaries is subjected to pure shear (see Fig. 5)

$$\dot{\sigma}_{11} = -\dot{\sigma}_{22} = (C_{11} - C_{12})\dot{\epsilon}_0 \tag{12}$$

Here, C_{ij} are the elastic constants. The crystal contains a single dislocation source on a slip plane that is inclined by 45° with each of the loading directions. This is a special case as it nicely isolates the contribution of core forces in that dislocation climb cannot occur unless the core fields are accounted for. The external applied load acts only tangentially to the slip system and does not contribute to the climb component of the Peach–Koehler force. Similarly, the Volterra fields from dislocations gliding on the same slip plane contribute only to the glide component of the Peach–Koehler force. Thus, a dislocation
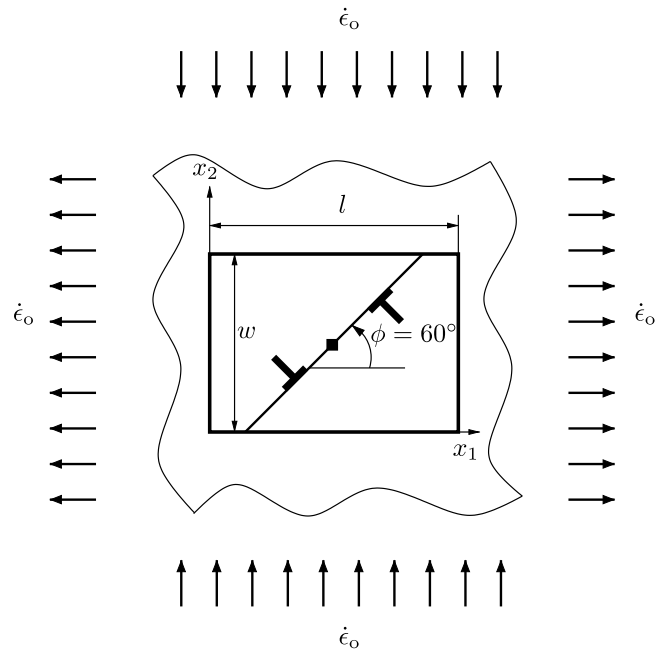

Fig. 5. Schematic representation of shear loading on a infinite body containing a dislocation source on a slip plane oriented at 45°. A dislocation dipole is also indicated.
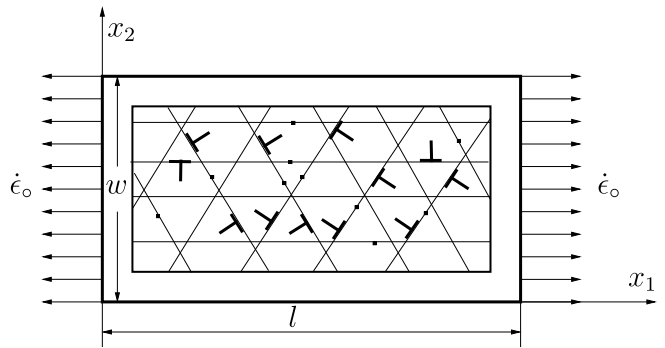

Fig. 6. Schematic representation of a thin film loaded in tension. The slip plane, the nucleation sources and the dislocations formed are also indicated.

on a plane with this orientation, when subjected to pure shear, can experience climb only if it originates from the core fields of neighboring dislocations. However, once an initial dislocation has climbed out of the slip plane, the other dislocations can contribute to further climb through the Volterra fields.

CASE 2. The only difference with CASE 1 is that the slip plane is inclined by 60° with the x_1− direction instead of 45°. In contrast to CASE 1, a dislocation on a plane with this orientation, will experience climb from the external applied load. Thus, the initial climb can originate from the dislocation core fields and/or the external load.

CASE 3. A single crystal thin film with length $l = 2.5$ and length to width ratio $l/w = 2.5$ is strained under tension in the x_1 direction; a schematic representation of the film is shown in Fig. 6.

The thin film has passivation layers of thickness $0.1w$ on all its surfaces. The passivation layers have the same elastic properties as the crystal but are made impenetrable to the dislocations. The thin film contains a source density of $25/\mu m^2$. Sources are uniformly distributed on three slip systems that are oriented at 0°, 60° and 120° with the x_1-axis, which is representative of an FCC crystal.

For the Cases 1–3, the stress–strain response of the crystals to loading is evaluated in terms of nominal stress

$$\sigma_{\text{nom}} = \frac{1}{w} \int_0^w \sigma_{11}(x_1 = l) \mathrm{d}x_2 \tag{13}$$

versus nominal strain,

$$\varepsilon_{\text{nom}} = \frac{u(x_1 = l, x_2 = 0) - u(x_1 = 0, x_2 = 0)}{l}. \tag{14}$$

To evaluate the effect of core fields on 2-D DDP simulations, we consider the following possible scenarios:

(i) glide$^{\text{Vol}}$ – no climb: climb is not allowed by setting $B_g/B_c \approx 0$ and dislocations are described only through Volterra fields.

(ii) glide$^{\text{Vol+core}}$ – no climb: climb is not allowed and the core fields are used along with the Volterra fields in the description of the dislocations, and therefore in the computation of the glide component of the Peach–Koehler force. This particular case is chosen to demonstrate the effect of core forces in the glide direction.

(iii) glide$^{\text{Vol}}$ - climb$^{\text{Vol}}$: climb is active and only the Volterra fields are used in the description of the dislocations.

(iv) glide$^{\text{Vol+core}}$ - climb$^{\text{Vol+core}}$: climb is active, both Volterra and core fields are considered in the description of dislocations.

4. Results

4.1. CASE 1

The crystal is strained to $\varepsilon_{\text{nom}} = 0.02$, at a strain rate of 1000/s. The stress–strain response and the increase in dislocation density are presented in Fig. 7. As expected, the stress–strain response shown in Fig. 7a is the same if the dislocations are not allowed to climb or if they can climb owing only to the Volterra fields. This is because the climb component of the Peach–Koehler force due to the Volterra fields of dislocations aligned on the same slip plane is zero for the current orientation of the slip system. In all the cases, the dislocations nucleate from the single Frank–Read source, glide on the slip plane and pile-up against the impenetrable wall. Also, the differences between the curves are negligible for the cases where the dislocations can glide due to the Volterra fields only or due to both Volterra and core fields. However, when the dislocations can also climb due to the core fields, the crystal presents a softer stress–strain response. Consistently, in Fig. 7b one can see that the crystal has the highest dislocation density when the component of climb from both the core fields are accounted for.

The effect of core fields on the distribution of stresses resolved along the slip plane and perpendicular to the slip plane are illustrated,

together with the corresponding dislocation structure, at an applied nominal strain $\varepsilon_{\text{nom}} = 0.02$ in Fig. 8. For the case without the core fields (i.e Fig. 8a and Fig. 8b), two long and dense dislocation pile-ups form against the impenetrable boundaries. These pile-ups cause a strong back-stress on the nucleation source, thereby leading to the strain hardening observed in Fig. 7a. Fig. 8c and Fig. 8d illustrate that by allowing climb due to both Volterra and core fields (glide$^{\text{Vol+ core}}$ - climb$^{\text{Vol+ core}}$), the dislocation pile-ups vanish. As a result, the response of the material is also much softer. This is because, by adding the core fields the dislocations climb on to neighboring slip planes. Once the initial dislocations have climbed due to the core fields, the Volterra fields take over and push them further away. This leads to a significant reduction of the back-stress created by the dislocation pile-ups on the source and allows for additional plastic deformation.

In Fig. 9, the ratio of Volterra and core components to the total climb force is presented for each dislocation leaving the original slip plane in the simulation where the dislocations climb due to both Volterra and core fields (glide$^{\text{Vol+ core}}$ - climb$^{\text{Vol+ core}}$). It is apparent that with increasing dislocation density the Volterra fields, which are long ranged, prevail over the short ranged core fields.

The effect of core fields is also evaluated for a copper lattice, where $M_1 = 1.2$ N, $M_2 = 0.6$ N and $b = 0.215$ nm. The trend is found to be identical to the case of an aluminum crystal and thus is not shown here.

4.1.1. CASE 2

As can be seen in Fig. 10, the stress–strain response of the crystal for all the simulations that include climb showed the same extent of softening irrespective of whether the climb is driven only by Volterra fields, or both the Volterra and core fields. Similarly, the dislocation density is higher for all cases that include climb.

The effect of core fields on the distribution of stresses resolved along the slip plane and perpendicular to the slip plane are illustrated along with the corresponding dislocation structure at an applied nominal strain $\varepsilon_{\text{nom}} = 0.02$ in Fig. 11. From these figures, it is clear that as long as the climb mechanism is active the dislocation pile-ups break loose and disappear. Again, irrespective of whether Volterra fields (glide$^{\text{Vol}}$ - climb$^{\text{Vol}}$) or both the Volterra and core fields (glide$^{\text{Vol+ core}}$ - climb$^{\text{Vol+ core}}$) are considered, the final dislocation structure is similar. This is an indication that the contribution of core fields to the dislocation climb is insignificant and can safely be neglected for the cases where the contribution from Volterra fields and/or applied loading are present.
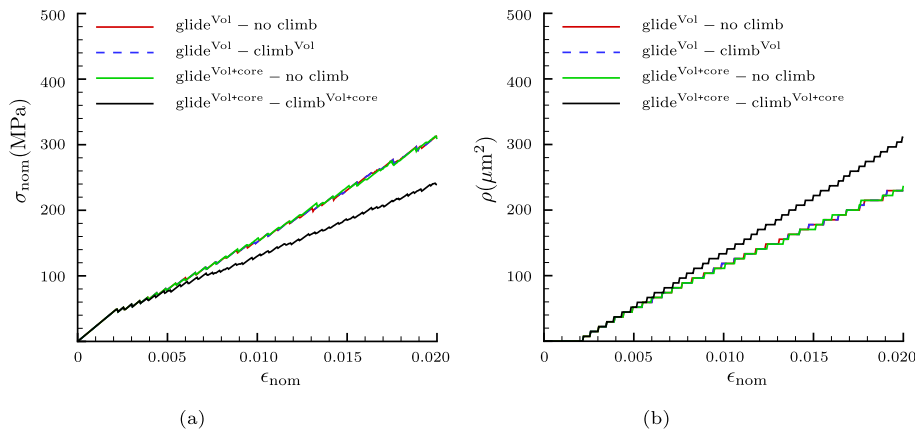

(a)

(b)

Fig. 7. Case 1: Pure shear of a crystal embedded in an infinite solid containing a source on a slip plane oriented at 45° with the x_1- axis. (a) Nominal stress σ_{nom} and (b) increase of the dislocation density ρ_{disl} during loading. The motion of the dislocations is assumed to be a result of either pure glide: glide$^{\text{Vol}}$ – no climb and glide$^{\text{Vol+ core}}$ – no climb; or a combination of glide and climb: glide$^{\text{Vol}}$ - climb$^{\text{Vol}}$ and glide$^{\text{Vol+ core}}$ - climb$^{\text{Vol+ core}}$.
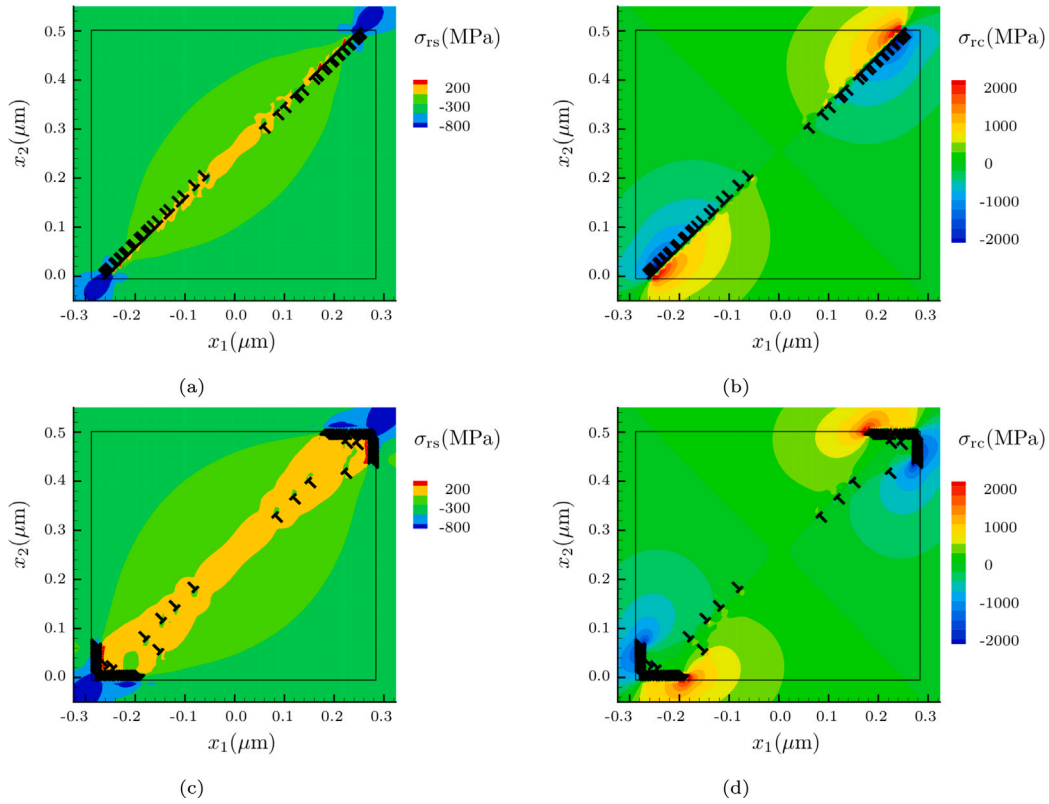
Fig. 8. Case1: (a) shear stress resolved on the slip plane, σ_{rs}, and (b) perpendicular to the slip plane, σ_{rc}, for the simulation where dislocations are only described through the Volterra fields (glide^{Vol} - climb^{Vol}); (c) shear stress resolved on the slip plane, σ_{rs}, and (d) perpendicular to the slip plane, σ_{rc}, for the simulation where dislocations are described through both Volterra and core fields (glide$^{Vol+ core}$ - climb$^{Vol+ core}$). The applied nominal strain is $\varepsilon_{nom} = 0.02$.
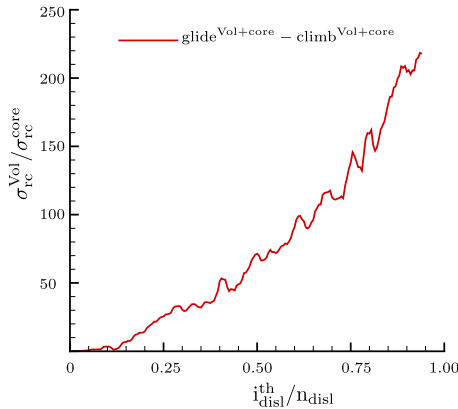

Fig. 9. The ratio of the Volterra to the core component of the total climb force, acting on each dislocation (i_{disl}^{th}) leaving the original slip plane. n_{disl} is the total number of dislocations that have climbed out of the original slip plane. The data points are connected through a continuous line as guide to the eye.

4.1.2. CASE 3

The thin film is loaded in tension at a strain rate of 1000/s. The stress–strain response and the increase in the dislocation density are presented in Fig. 12 as average over ten realizations. These realizations differ only in the location and strength of the sources which are taken out of a normal distribution with a mean source strength = 50 MPa and standard deviation of 10 MPa. The stress–strain response is in line

with that observed in CASE 2: allowing for climb leads to a significant decrease in strain hardening.

The effect of core fields on the distribution of stresses resolved along the 60° slip plane and perpendicular to the 60° slip plane are illustrated along with the corresponding dislocation structure at an applied nominal strain $\varepsilon_{nom} = 0.02$ in Fig. 13.

It is indeed possible to see from these figures that as long as dislocation climb is allowed, dislocations travel long distances away from their original planes and accumulate along the impenetrable boundaries. Also, we see dislocations walls forming especially with dislocations on the horizontal slip planes, which is a low energy configuration. Additionally, the dislocation structure is only mildly affected when climb is also driven by the core fields. This again confirms that the contribution of core fields to the dislocation climb can safely be neglected for the cases where the contribution from Volterra fields and/or an external loading inducing climb are present.

Simulations were performed also for thin films with smaller dimensions, but not reported here for brevity. The expected size effect was found, less pronounced when climb was allowed, but no significant effect of core fields.

5. Conclusions

In this work simulations are performed to assess whether and to which extent accounting for dislocation core fields in the description of dislocations affects the results of dislocation dynamics simulations. This study demonstrates that the contribution of the core fields in determining the plastic response of crystals under loading modeled through 2D-DDP is negligible: it does neither affect significantly the
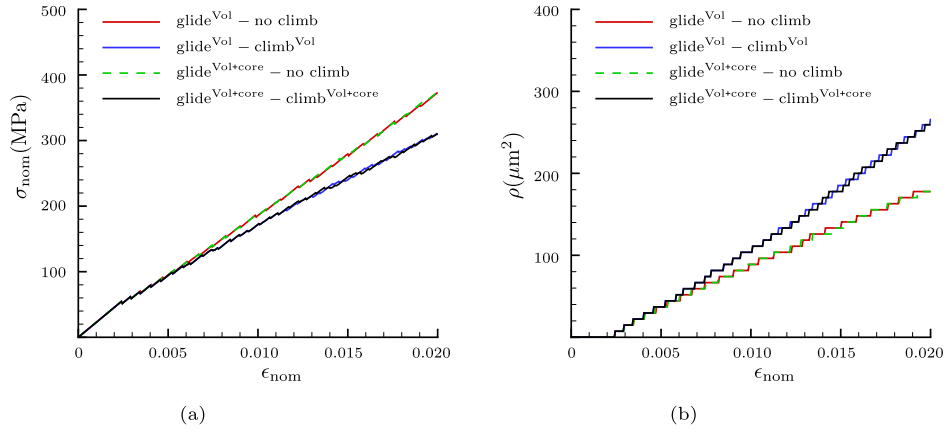
Fig. 10. Case 2: Pure shear of a crystal embedded in an infinite solid containing a source on a slip plane oriented at 60° with the x_1- axis. (a) Nominal stress σ_{nom} and (b) increase of the dislocation density ρ_{disl} during loading. The motion of the dislocations is assumed to be a result of either pure glide: glide$^{\text{Vol}}$ – no climb and glide$^{\text{Vol+ core}}$ – no climb; or a combination of glide and climb: glide$^{\text{Vol}}$ - climb$^{\text{Vol}}$ and glide$^{\text{Vol+ core}}$ - climb$^{\text{Vol+ core}}$.
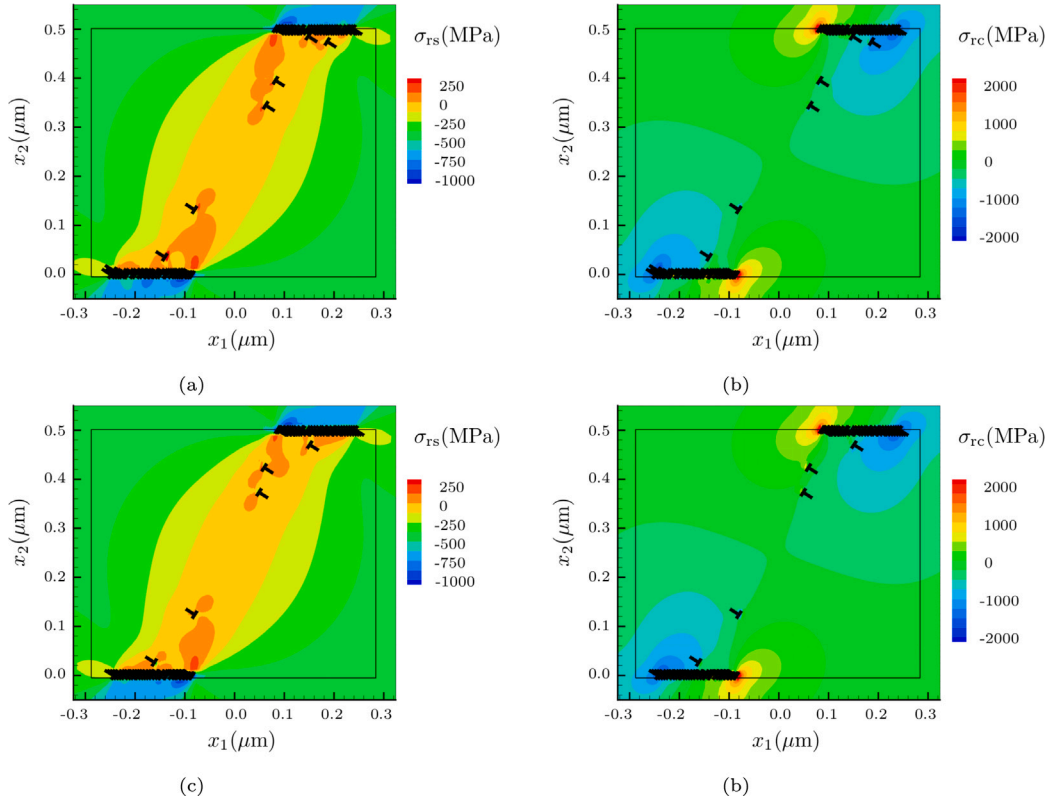
Fig. 11. Case 2: (a) shear stress resolved on the slip plane, σ_{rs}, and (b) perpendicular to the slip plane, σ_{rc}, for the simulation where dislocations are only described through the Volterra fields (glide$^{\text{Vol}}$ - climb$^{\text{Vol}}$); (c) shear stress resolved on the slip plane, σ_{rs}, and (d) perpendicular to the slip plane, σ_{rc}, for the simulation where dislocations are described through both Volterra and core fields (glide$^{\text{Vol+ core}}$ - climb$^{\text{Vol+ core}}$). The applied nominal strain is $\varepsilon_{\text{nom}} = 0.02$.

stress–strain response, nor the evolution of the dislocation distribution. This is because dislocation climb is driven at small dislocation densities by the external load resolved normal to the slip plane, and at large densities also by the Volterra stress field of the dislocations. The only special case we found where adding core to Volterra fields leads to completely different results than considering Volterra fields alone, is the extremely simplified scenario where a crystal under pure shear contains only a dislocation source on a slip plane oriented at 45° with the loading direction.

Therefore, we can conclude that the core effects can be neglected in problems where plasticity is driven by glide and climb of edge dislocations that can be modeled by 2D-DDP. The conclusions of this work cannot however be extended to 3D-DDP, given that in three dimensions core fields might affect junction formation between dislocation loops. Additionally, core fields could alter the formation and propagation of partial dislocations, which are not modeled in the two-dimensional framework. The effect of core fields on the dynamics of three-dimensional dislocation networks can be an interesting avenue for future research.
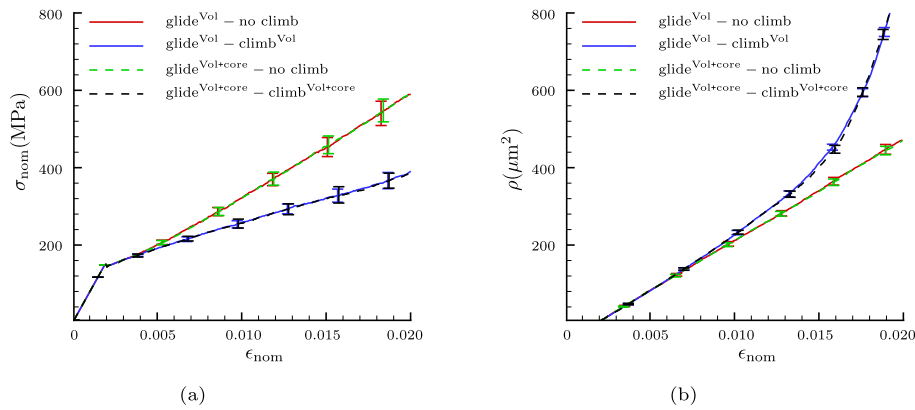
Fig. 12. Case 3: Stress–strain response of a thin film with multiple sources and obstacles distributed on three sets of slip planes oriented at 0°, 60° and 120° (a) Nominal stress σ_{nom} and (b) increase of the dislocation density ρ_{disl} during loading. The motion of dislocations are assumed to be a result of pure glide: (glide$^{\mathrm{Vol}}$ – no climb) and (glide$^{\mathrm{Vol+ core}}$ – no climb). A combination of glide and climb: (glide$^{\mathrm{Vol}}$ - climb$^{\mathrm{Vol}}$) and (glide$^{\mathrm{Vol+ core}}$ - climb$^{\mathrm{Vol+ core}}$).

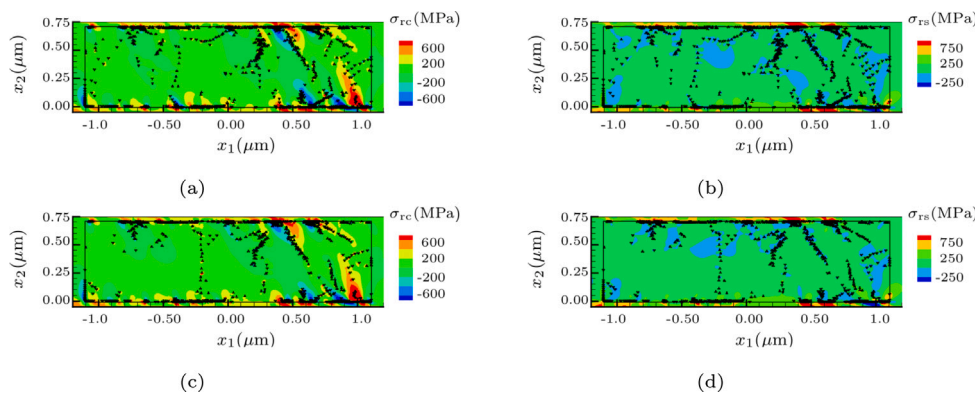**Fig. 13.** Case 3: Distribution of the resolved shear stress (a) along the slip plane oriented at 60° with the loading direction, σ_{rs}, and (b) perpendicular to it (σ_{rc}) for simulations accounting for Volterra fields only (glide$^{\mathrm{Vol}}$ - climb$^{\mathrm{Vol}}$); Distribution of the resolved shear stress (c) along the slip plane oriented at 60° with the loading direction, σ_{rs}, and (d) perpendicular to it (σ_{rc}) for simulations accounting for both Volterra and core fields (glide$^{\mathrm{Vol+ core}}$ - climb$^{\mathrm{Vol+ core}}$). The applied nominal strain is $\epsilon_{\mathrm{nom}} = 0.02$.

Declaration of competing interest

One or more of the authors of this paper have disclosed potential or pertinent conflicts of interest, which may include receipt of payment, either direct or indirect, institutional support, or association with an entity in the biomedical field which may be perceived to have potential conflict of interest with this work. For full disclosure statements refer to https://doi.org/10.1016/j.mechmat.2021.104137.. Lucia Nicola reports financial support was provided by European Research Council.

References

Amodeo, R.J., Ghoniem, N.M., 1990. Dislocation dynamics. I. A proposed methodology for deformation micromechanics. Phys. Rev. B 41, 6958–6967. http://dx.doi.org/10.1103/PhysRevB.41.6958, URL https://link.aps.org/doi/10.1103/PhysRevB.41.6958.

Ayas, C., Dautzenberg, L.C.P., Geers, M.G.D., Deshpande, V.S., 2015. Climb-enabled discrete dislocation plasticity analysis of the deformation of a particle reinforced composite. J. Appl. Mech. 82 (7), 071007. http://dx.doi.org/10.1115/1.4030319, arXiv:https://asmedigitalcollection.asme.org/appliedmechanics/article-pdf/82/7/071007/6081230/jam_082_07_071007.pdf.

Ayas, C., Deshpande, V., Geers, M., 2012. Tensile response of passivated films with climb-assisted dislocation glide. J. Mech. Phys. Solids 60 (9), 1626–1643.

Ayas, C., van Dommelen, J., Deshpande, V., 2014. Climb-enabled discrete dislocation plasticity. J. Mech. Phys. Solids 62, 113–136.

Chang, H.-J., Segurado, J., Molina-Aldareguía, J.M., Soler, R., LLorca, J., 2016. A 3D dislocation dynamics analysis of the size effect on the strength of [1 1 1] LiF micropillars at 300K and 600K. Modelling Simulation Mater. Sci. Eng. 24, 035009.

Clouet, E., 2011. Dislocation core field. I. Modeling in anisotropic linear elasticity theory. Phys. Rev. B 84, 224111.

Clouet, E., Ventelon, L., Willaime, F., 2009. Dislocation core energies and core fields from first principles. Phys. Rev. Lett. 102, 055502.

Danas, K., Deshpande, V., 2013. Plane-strain discrete dislocation plasticity with climb-assisted glide motion of dislocations. Modelling Simulation Mater. Sci. Eng. 21 (4), 045008.

Davoudi, K.M., Nicola, L., Vlassak, J.J., 2012. Dislocation climb in two-dimensional discrete dislocation dynamics. J. Appl. Phys. 111 (10), 103522.

der Giessen, E.V., Needleman, A., 1995. Discrete dislocation plasticity: a simple planar model. Modelling Simulation Mater. Sci. Eng. 3 (5), 689–735.

Deshpande, V., Needleman, A., der Giessen, E.V., 2003. Discrete dislocation plasticity modeling of short cracks in single crystals. Acta Mater. 51 (1), 1–15.

Eshelby, J., Read, W., Shockley, W., 1953. Anisotropic elasticity with applications to dislocation theory. Acta Metall. 1 (3), 251–259.

Fan, H., Li, Z., Huang, M., 2012. Toward a further understanding of intermittent plastic responses in the compressed single/bicrystalline micropillars. Scr. Mater. 66, 813–816.

Fivel, M., Verdier, M., Canova, G., 1997. 3D simulation of a nanoindentation test at a mesoscopic scale. Mater. Sci. Eng. A 234–236, 923–926.

Gehlen, P., Hirth, J., Hoagland, R., Kanninen, M., 1972. A new representation of the strain field associated with the cube-edge dislocation in a model of a α-iron. J. Appl. Phys. 43 (10), 3921–3933.

Ghoniem, N.M., Sun, L.Z., 1999. Fast-sum method for the elastic field of three-dimensional dislocation ensembles. Phys. Rev. B 60, 128–140.

Ghoniem, N.M., Tong, S.-H., Sun, L.Z., 2000. Parametric dislocation dynamics: A thermodynamics-based approach to investigations of mesoscopic plastic deformation. Phys. Rev. B 61, 913–927.

Henager, C.H., Hoagland, R.G., 2000. Forces between dislocations due to dislocation core fields. MRS Proc. 652, Y7.7.

Henager, Jr., C.H., Hoagland, R.G., 2005. Dislocation and stacking fault core fields in fcc metals. Phil. Mag. 85 (36), 4477–4508.

Hirth, J.P., Lothe, J., 1968. Theory of Dislocations. McGraw-Hill, New York.

Huang, M., Liang, S., Li, Z., 2017. An extended 3D discrete-continuous model and its application on single- and bi-crystal micropillars. Modelling Simulation Mater. Sci. Eng. 25, 035001.

Kuan, H., Hirth, J., 1976. Dislocation pileups near the interface of a bimaterial couple. Mater. Sci. Eng. 22, 113–131.

Kubin, L.P., Canova, G., Condat, M., Devincre, B., Pontikis, Y., 1992. Dislocation microstructures and plastic flow: a 3D simulation. Solid State Phenom. 23–24, 455–472.

Nabarro, F.R.N., 1967. Theory of Crystal Dislocations. Oxford U. P., Oxford.

Nicola, L., Van der Giessen, E., Needleman, A., 2003. Discrete dislocation analysis of size effects in thin films. J. Appl. Phys. 93 (10), 5920–5928.

Nicola, L., Xiang, Y., Vlassak, J., der Giessen, E.V., Needleman, A., 2006. Plastic deformation of freestanding thin films: Experiments and modeling. J. Mech. Phys. Solids 54 (10), 2089–2110.

Peng, S., Wei, Y., Jin, Z., Yang, W., 2019. Supersonic screw dislocations gliding at the shear wave speed. Phys. Rev. Lett. 122, 045501. http://dx.doi.org/10.1103/PhysRevLett.122.045501, URL https://link.aps.org/doi/10.1103/PhysRevLett.122.045501.

Reddy, G.P., Robertson, C., Déprés, C., Fivel, M., 2013. Effect of grain disorientation on early fatigue crack propagation in face-centred-cubic polycrystals: A three-dimensional dislocation dynamics investigation. Acta Mater. 61 (14), 5300–5310.

Rice, J.R., 1987. Tensile crack tip fields in elastic-ideally plastic crystals. Mech. Mater. 6 (4), 317–335. http://dx.doi.org/10.1016/0167-6636(87)90030-5.

Shin, C., Fivel, M., Verdier, M., Robertson, C., 2005. Dislocation dynamics simulations of fatigue of precipitation-hardened materials. Mater. Sci. Eng. A 400–401, 166–169.

Venugopalan, S., Nicola, L., 2019. Indentation of a plastically deforming metal crystal with a self-affine rigid surface: A dislocation dynamics study. Acta Mater. 165, 709–721. http://dx.doi.org/10.1016/j.actamat.2018.10.020, URL https://www.sciencedirect.com/science/article/pii/S1359645418308127.

Walker, A.M., Gale, J.D., Slater, B., Wright, K., 2005a. Atomic scale modelling of the cores of dislocations in complex materials part 1: methodology. Phys. Chem. Chem. Phys. 7 (17), 3227–3234.

Walker, A.M., Gale, J.D., Slater, B., Wright, K., 2005b. Atomic scale modelling of the cores of dislocations in complex materials part 2: applications. Phys. Chem. Chem. Phys. 7, 3235–3242.

Wei, Y., Peng, S., 2017. The stress-velocity relationship of twinning partial dislocations and the phonon-based physical interpretation. Sci. China Phys. Mech. Astron. 60 (11), 1869–1927. http://dx.doi.org/10.1007/s11433-017-9076-8, URL https://doi.org/10.1007/s11433-017-9076-8.

Wei, D., Zaiser, M., Feng, Z., Kang, G., Fan, H., Zhang, X., 2019. Effects of twin boundary orientation on plasticity of bicrystalline copper micropillars: A discrete dislocation dynamics simulation study. Acta Mater. 176, 289–296.

Weygand, D., Friedman, L.H., der Giessen, E.V., Needleman, A., 2002. Aspects of boundary-value problem solutions with three-dimensional dislocation dynamics. Modelling Simulation Mater. Sci. Eng. 10, 437–468.

Wu, R., Zaiser, M., 2020. Cell structure formation in a two-dimensional density-based dislocation dynamics model. arXiv:1803.05951.

Xia, S.X., El-Azab, A., 2015. A preliminary investigation of dislocation cell structure formation in metals using continuum dislocation dynamics. IOP Conf. Ser. Mater. Sci. Eng. 89, 012053.

Yang, M., Pan, Y., Yuan, F., Zhu, Y., Wu, X., 2016. Back stress strengthening and strain hardening in gradient structure. Mater. Res. Lett. 4 (3), 145–151. http://dx.doi.org/10.1080/21663831.2016.1153004.

Zhang, Y., Gao, Y., Nicola, L., 2014. Lattice rotation caused by wedge indentation of a single crystal: Dislocation dynamics compared to crystal plasticity simulations. J. Mech. Phys. Solids 68, 267–279.